Lung and Kidney ACE2 and TMPRSS2 in Renin-Angiotensin System Blocker–Treated Comorbid Diabetic Mice Mimicking Host Factors That Have Been Linked to Severe COVID-19

Sri Nagarjun Batchu,[1] Harmandeep Kaur,[1] Veera Ganesh Yerra,[1] Suzanne L. Advani,[1] M. Golam Kabir,[1] Youan Liu,[1] Thomas Klein,[2] and Andrew Advani[1]

Diabetes 2021;70:759–771 | https://doi.org/10.2337/db20-0765

The causes of the increased risk of severe coronavirus disease 2019 (COVID-19) in people with diabetes are unclear. It has been speculated that renin-angiotensin system (RAS) blockers may promote COVID-19 by increasing ACE2, which severe acute respiratory syndrome coronavirus 2 uses to enter host cells, along with the host protease TMPRSS2. Taking a reverse translational approach and by combining in situ hybridization, primary cell isolation, immunoblotting, quantitative RT-PCR, and liquid chromatography–tandem mass spectrometry, we studied lung and kidney ACE2 and TMPRSS2 in diabetic mice mimicking host factors linked to severe COVID-19. In healthy young mice, neither the ACE inhibitor ramipril nor the AT1 receptor blocker telmisartan affected lung or kidney ACE2 or TMPRSS2, except for a small increase in kidney ACE2 protein with ramipril. In contrast, mice with comorbid diabetes (aging, high-fat diet, and streptozotocin-induced diabetes) had heightened lung ACE2 and TMPRSS2 protein levels and increased lung ACE2 activity. None of these parameters were affected by RAS blockade. ACE2 was similarly upregulated in the kidneys of mice with comorbid diabetes compared with aged controls, whereas TMPRSS2 (primarily distal nephron) was highest in telmisartan-treated animals. Upregulation of lung ACE2 activity in comorbid diabetes may contribute to an increased risk of severe COVID-19. This upregulation is driven by comorbidity and not by RAS blockade.

When severe acute respiratory syndrome coronavirus 2 (SARS-CoV-2) emerged in December 2019, early reports suggested that people with diabetes were at an increased risk of adverse outcomes, including admission to the intensive care unit, mechanical ventilation, and death (1–3). These initial insights have subsequently been confirmed by larger epidemiological surveys. For instance, in a whole-population study from England that included data from 61,414,470 individuals and 23,698 in-hospital coronavirus disease 2019 (COVID-19)–related deaths, the odds ratio (95% CI) for death as a result of COVID-19 was 3.51 (3.16–3.90) for people with type 1 diabetes and 2.03 (1.97–2.09) for people with type 2 diabetes (4). The cause of this increase in risk for people with diabetes remains, however, unclear.

SARS-CoV-2 enters host cells by binding to its receptor ACE2 (5–8), a type I transmembrane carboxypeptidase. Ordinarily, ACE2 plays a counterbalancing role within the renin-angiotensin system (RAS) by hydrolyzing angiotensin II (Ang II) to form Ang 1–7 (9) and by cleaving Ang I to form Ang 1–9, which itself can subsequently be hydrolyzed by ACE to form Ang 1–7 (10). The actions of ACE2 have been generally well characterized in the kidneys, which, like the lungs, are susceptible to direct viral infection by SARS-CoV-2 (11). In the kidneys of diabetic mice, ACE2 protein (but not mRNA) is upregulated in renal tubules (12,13), although not in glomeruli (14). In contrast, comparatively little is known about the effect of diabetes on lung ACE2, although it is noteworthy that under normal circumstances, ACE2 expression and activity are substantially lower in the lungs than they are in the kidneys (15). It

[1]Keenan Research Centre for Biomedical Science and Li Ka Shing Knowledge Institute, St. Michael's Hospital, Toronto, Ontario, Canada
[2]Department of Cardiometabolic Diseases Research, Boehringer Ingelheim Pharma, Biberach, Germany

Corresponding author: Andrew Advani, andrew.advani@unityhealth.to

Received 24 July 2020 and accepted 27 November 2020

This article contains supplementary material online at https://doi.org/10.2337/figshare.13342160.

S.N.B., H.K., and V.G.Y. contributed equally to this work.

This article is part of a special article collection available at https://diabetes.diabetesjournals.org/collection/diabetes-and-COVID19-articles.

has also been postulated that use of ACE inhibitors or Ang II type 1 receptor blockers (ARBs) could increase the risk of COVID-19 in diabetes by causing a compensatory upregulation in ACE2 either by blocking the conversion of Ang I to Ang II or by preventing the binding of Ang II to Ang II type 1 receptor, respectively, thus facilitating viral entry (16). Yet, contrary to this hypothesis, a recent study found no increase in lung or kidney ACE2 when RAS blocker therapy was administered to healthy mice (17). Presence and abundance of a cognate receptor are not, however, the sole host factors that influence coronavirus cellular and tissue tropism. Following receptor engagement by the viral surface spike glycoprotein (S protein), entry into the cell is facilitated by cleavage of the viral S protein by host cell surface proteases, allowing fusion of the viral and host cell membranes (18). Several different host proteases can perform this function, but the best characterized for SARS-CoV-2 is the type 2 transmembrane serine protease transmembrane protease serine 2 (TMPRSS2) (18).

In the current study, we reasoned that a reverse translational approach was well suited to better understanding how host factors related to SARS-CoV-2 infection may be affected by comorbidities or treatments that have been linked to adverse COVID-19 outcomes. Recognizing that aged people with diabetes, who are commonly prescribed RAS blockers, are at increased risk of adverse COVID-19 outcomes, we studied the expression patterns of ACE2 and TMPRSS2 in a mouse model that mimics this endophenotype (19).

RESEARCH DESIGN AND METHODS

Study 1

Male C57BL/6N mice (C57BL/6NCrl; Charles River Laboratories, Senneville, Quebec, Canada) aged 7–8 weeks were randomly allocated to receive standard drinking water or drinking water supplemented with either the ACE inhibitor ramipril (10 mg/kg/day) (#15558; Cayman Chemical, Ann Arbor, MI) or the ARB telmisartan (3 mg/kg/day) (#11615; Cayman Chemical) in 0.1% DMSO (20,21). After 1 week, systolic blood pressure (SBP) was recorded using a CODA noninvasive blood pressure system (Kent Scientific, Torrington, CT) (22), and tissues were harvested.

Study 2

In a separate substudy, male C57BL/6N mice (Charles River Laboratories) aged 7–8 weeks were randomly allocated to treatment with ramipril (10 mg/kg/day) or telmisartan (3 mg/kg/day) in drinking water or drinking water alone for 1 week. Primary type II pneumocytes were isolated from lungs by combining mechanical and enzymatic digestion using digestion mix containing 2 mg/mL collagenase II (Worthington Biochemical Corp., Lakewood, NJ), 1.2 units/mL Dispase I (MilliporeSigma, Oakville, Ontario, Canada), and 5 units/mL DNase 1 (MilliporeSigma) at 37°C with gentle shaking for 45–60 min. Cells were filtered using a 40-μm filter and washed with PBS before incubating with epithelial cell adhesion molecule (#130-117-751; Miltenyi Biotec, Somerville, MA) and surfactant protein C (#bs-10378R-Biotin; Bioss Antibodies Inc., Woburn, MA) colabeled CELLection Dynabeads (#11533D; Thermo Fisher Scientific, Waltham, MA).

To confirm enrichment of lung primary cells for type II pneumocytes, we compared expression levels of the type II pneumocyte marker *Sftpc* (encoding surfactant protein C) between primary cells isolated from mouse lungs and a control primary cell population not expected to express *Sftpc* (i.e., primary kidney fibroblasts). To isolate primary kidney fibroblasts, male C57BL/6N mice (Charles River Laboratories) aged 8–10 weeks underwent unilateral ureteral obstruction surgery. In brief, under 2% isoflurane anesthesia, an incision was made in the left flank, and two 5-0 silk sutures were used to occlude the left ureter just distal to its origin. After 7 days, kidneys were harvested and fibroblasts isolated on the basis of a method adapted from that performed previously in mouse hearts (23), using digestion mix containing 2 mg/mL collagenase II (Worthington Biochemical) and 5 units/mL DNase 1 (MilliporeSigma) at 37°C with gentle shaking for 60–90 min. Cells were serially filtered using 70-μm and 40-μm filters and washed with PBS before plating for 1 h at 37°C and 5% CO_2 in DMEM containing 10% FBS, L-glutamine, and 1% penicillin/streptomycin. Adherent cells were washed thoroughly with PBS before RNA isolation.

Study 3

Male C57BL/6N mice (Charles River Laboratories) aged 7–8 weeks were fed a high-fat diet (HFD) (45% kcal fat, 35% kcal carbohydrate, and 0.05% w/w cholesterol; Research Diets Inc., New Brunswick, NJ). After 15 weeks, mice received a single intraperitoneal injection of streptozotocin (STZ) (90 mg/kg in 0.1 mol/L sodium citrate, pH 4.5) following a 4-h fast. Diabetes (blood glucose ≥12 mmol/L) was confirmed 2 weeks after STZ injection by blood glucose testing (OneTouch UltraMini; LifeScan Canada Ltd., Burnaby, British Columbia, Canada). Mice were maintained on an HFD for a further 21 weeks. After 19 weeks, mice were treated with either ramipril (10 mg/kg/day) or telmisartan (3 mg/kg/day) in drinking water or drinking water alone for the final 2 weeks of the study. Male age-matched controls were fed standard chow throughout the study period. Urine albumin excretion was determined using Albuwell M ELISA (Ethos Biosciences, Newtown Square, PA) after 24-h metabolic caging. Plasma cholesterol was measured using Cholesterol Quantitation Kit (MAK043; MilliporeSigma), and plasma triglycerides were measured using Triglyceride Colorimetric Assay Kit (#10010303; Cayman Chemical). For invasive blood pressure monitoring, mice were anesthetized, intubated, and artificially ventilated (1–2% isoflurane, tidal volume 300–350 μL, O_2 flow rate 2 L/min, 180–200 breaths/min). A pressure-volume catheter (Millar Mikro-Tip, 1.4F; AD Instruments, Colorado Springs, CO) was inserted and advanced into the ascending aorta for monitoring of aortic pressure (24). Data were acquired and analyzed using LabChart Pro

software (AD Instruments). All experimental procedures adhered to the guidelines of the Canadian Council of Animal Care and were approved by the St. Michael's Hospital Animal Care Committee.

In Situ Hybridization

In situ hybridization for *Ace2* and *Tmprss2* was performed with RNAscope (Advanced Cell Diagnostics, Hayward, CA) according to the manufacturer's instructions and using custom software as previously described (25), with probesets specific for *Ace2* (#417081) and *Tmprss2* (#496721); custom-designed sense probes for *Ace2* (#894471) and *Tmprss2* (#894481); and positive control probeset specific for *Polr2a* (#312471) and negative control probeset for *DapB* (#310043). Hybridization signals were detected using Fast Red, and RNA staining was identified as red puncta on light microscopy.

Immunoblotting

Immunoblotting of mouse lung and kidney homogenates was performed with the following antibodies: ACE2 1:1,000 (ab15348; Abcam, Cambridge, MA), TMPRSS2 1:1,000 (EPR3861, ab92323; Abcam), GAPDH 1:1,000 (#2118; Cell Signaling Technology, Danvers, MA), and β-actin 1:10,000 (A1978; MilliporeSigma). Densitometry was performed using ImageJ version 1.39 software (National Institutes of Health, Bethesda, MD). To determine the specificity of the ACE2 antibody, two nitrocellulose membranes loaded with identical samples were probed simultaneously. One membrane was incubated with 1:1,000 ab15348 anti-ACE2 antibody (10 μg in 10 mL 5% BSA prepared in Tris-buffered saline with Tween), and the other was probed with the same antibody at the same dilution preincubated with a 10-fold excess of the ACE2 immunizing peptide (CKGENNPGFQNTDDVQTSF; Bio Basic Inc., Markham, Ontario, Canada) for 5 h at 4°C and 2 h at 37°C.

Real-time Quantitative RT-PCR

RNA was isolated from snap frozen lung or kidney tissue or from isolated type II pneumocytes or kidney fibroblasts using TRIzol Reagent (Thermo Fisher Scientific), and RNA was reverse transcribed using a high-capacity cDNA reverse transcription kit (Thermo Fisher Scientific). Primer sequences (Integrated DNA Technologies, Coralville, IA) were as follows: *Ace2* forward 5′-TGATGAATCAGGGCTGGGATG-3′, reverse 5′-ATTCTGAAGTCTCCGTGTCCC-3′; *Tmprss2* forward 5′-GAGAACCGTTGTGTTCGTCTC-3′, reverse 5′-GCTCTGGTCT GGTATCCCTTG-3′; *Rpl13a* forward 5′-GCTCTCAAGGTTGTT CGGCTGA-3′, reverse 5′-AGATCTGCTTCTTCTTCCGATA-3′; *Sftpc* forward 5′-CGTTGTCGTGGTGATTG-3, reverse 5′-GTCA TACACAACGATGCC-3′; and *Gapdh* forward 5′-AGACGGCCG CATCTTCTT-3′, reverse 5′-TTCACACCGACCTTCACCAT-3′. SYBR green–based quantitative RT-PCR (qRT-PCR) was performed on a QuantStudio 7 Flex Real-Time PCR System (Thermo Fisher Scientific). Data analysis was performed using Applied Biosystems Comparative C_T method.

Glomerulosclerosis Index

Glomerulosclerosis was semiquantitatively evaluated from ~50 glomeruli on periodic acid Schiff–stained kidney sections from each mouse, as previously described (26).

Measurement of Endogenous Angiotensin Metabolites and ACE2 Activity in Mouse Lung Tissue

Angiotensin metabolites [Ang I (1–10), Ang II, Ang III (2–8), Ang IV (3–8), Ang 1–7, Ang 1–5] and ACE2 activity were quantified in mouse lung tissue using liquid chromatography–tandem mass spectrometry (LC-MS/MS) (Attoquant Diagnostics, Vienna, Austria) (Supplementary Material).

Statistics

Data are expressed as mean ± SD. Statistical significance was determined by one-way ANOVA with a Fisher least significant difference posttest, Kruskal-Wallis test with Dunn posttest, or two-tailed Student *t* test, as indicated. Statistical analyses were performed using GraphPad Prism 8 for macOS (GraphPad Software Inc., San Diego, CA). $P < 0.05$ was considered statistically significant.

Data and Resource Availability

The data sets generated and/or analyzed during the current study are available from the corresponding author upon reasonable request.

RESULTS

Site-Specific Expression Patterns of *Ace2* and *Tmprss2* Differ From Each Other in Mouse Lungs and Kidneys

We began by comparing the expression patterns of *Ace2* and *Tmprss2* in the lungs and kidneys of normal male mice (C57BL/6N mice aged ~10 weeks fed standard chow and drinking water). Using RNAscope in situ hybridization, we observed a predominant bronchiolar pattern of expression of *Ace2* in mouse lungs, with occasional staining for RNA transcript in scattered alveolar cells (Fig. 1*A*). In contrast, *Tmprss2* was more diffuse in its distribution, being equally present in both the bronchioles and the alveoli (Fig. 1*A*). In the kidney cortex, *Ace2* transcript was observed primarily within the kidney tubules, with greater probe labeling in the proximal tubules than in the distal tubules and cortical collecting ducts and only occasional transcripts present in glomerular cells (Fig. 1*B*). *Tmprss2* was also present in both the proximal tubules and the distal tubules and cortical collecting ducts of the kidney cortex but was expressed primarily within the cells of the distal nephron, with, again, sparse transcripts present within the glomeruli (Fig. 1*B*). Notably, *Tmprss2* riboprobe binding was especially prominent within the transitional epithelium lining the renal papilla (Fig. 1*B*). Because acute myocardial injury may also occur in severe COVID-19 (27), we also took the opportunity to probe for *Ace2* and *Tmprss2* in mouse hearts. However, both transcripts were barely detectable in mouse cardiac tissue in contrast to either the lungs or the kidneys (Fig. 1*C* and *D*).

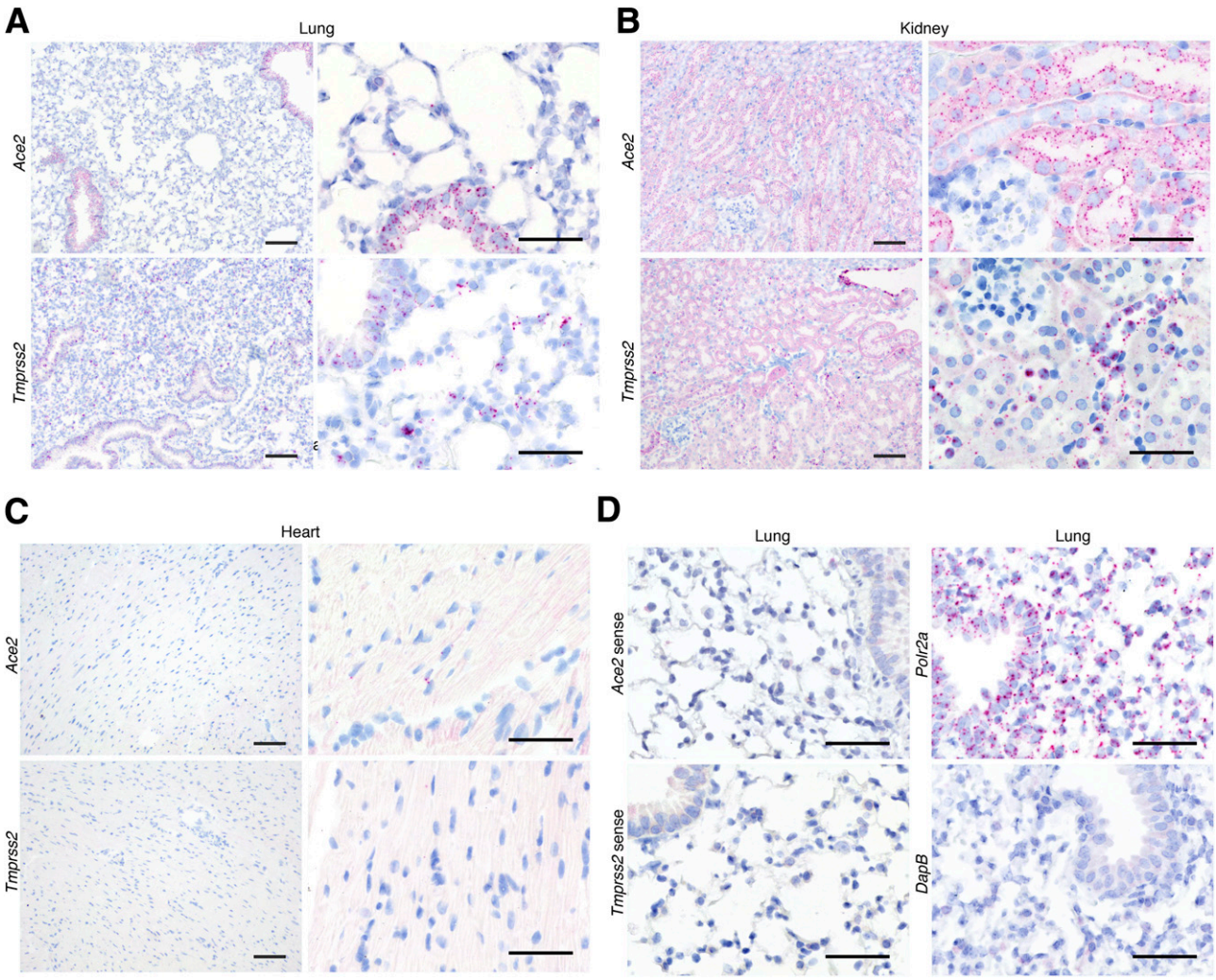

Figure 1—Site-specific localization of *Ace2* and *Tmprss2* in mouse lungs, kidneys, and heart using RNAscope in situ hybridization. *A*: *Ace2* or *Tmprss2* in mouse lung (left magnification ×100 [scale bars = 100 μm], right magnification ×400 [scale bars = 50 μm]). *B*: *Ace2* or *Tmprss2* in mouse kidney (left magnification ×100 [scale bars = 100 μm], right magnification ×400 [scale bars = 50 μm]). In the kidney sections, *Ace2* transcripts are predominantly seen within the proximal tubule cells of the kidney cortex, which can be recognized by their taller appearance, eosinophilic cytoplasm, and brush border. *Tmprss2* transcripts are most abundant in the distal convoluted tubules (flatter, paler cells) and cortical collecting ducts as well as in the transitional epithelium lining the renal papilla (evident in the top right-hand corner of the ×100 magnification image). *C*: *Ace2* or *Tmprss2* in mouse heart (left magnification ×100 [scale bars = 100 μm], right magnification ×400 [scale bars = 50 μm]). *D*: Sense probes for *Ace2* and *Tmprss2* and positive (*Polr2a*) and negative (bacterial transcript *DapB*) controls in mouse lung (magnification ×400 [scale bars = 50 μm]).

Neither ACE Inhibition nor AT1 Receptor Blockade Affect ACE2 or TMPRSS2 Expression in the Lungs of Young, Otherwise Healthy Mice

We examined ACE2 protein levels in mouse lungs and kidneys using a rabbit polyclonal ACE2 antibody (ab15348). To test the specificity of the ACE2 antibody, we preincubated the antibody with chemically synthesized immunizing peptide, affirming previous observations (15) that ACE2 protein levels are notably higher in the kidneys than the lungs (Fig. 2). We treated male C57BL/6N mice with standard drinking water or drinking water containing the ACE inhibitor ramipril or the ARB telmisartan. Body weight did not differ between treatment groups (Fig. 3*A*). Either ramipril or telmisartan significantly lowered SBP, with the magnitude of SBP lowering being higher with the 10 mg/kg/day dose of ramipril than the 3 mg/kg/day dose of telmisartan (Fig. 3*B*). By immunoblotting (Fig. 3*C* and *D*) and qRT-PCR (Fig. 3*E* and *F*), we observed that neither ramipril nor telmisartan treatment affected either lung ACE2 or TMPRSS2 expression. In mouse kidneys, we observed a small, but statistically significant increase in ACE2 protein levels following ramipril treatment (Fig. 3*G*), without change in TMPRSS2 (Fig. 3*H*). Transcript levels for either *Ace2* or *Tmprss2* did not differ between the treatment groups (Fig. 3*I* and *J*). Of note, ACE2 protein appeared as a doublet upon immunoblotting of mouse lung homogenates but not mouse kidney homogenates, as has been reported previously under some other experimental conditions (28–30).

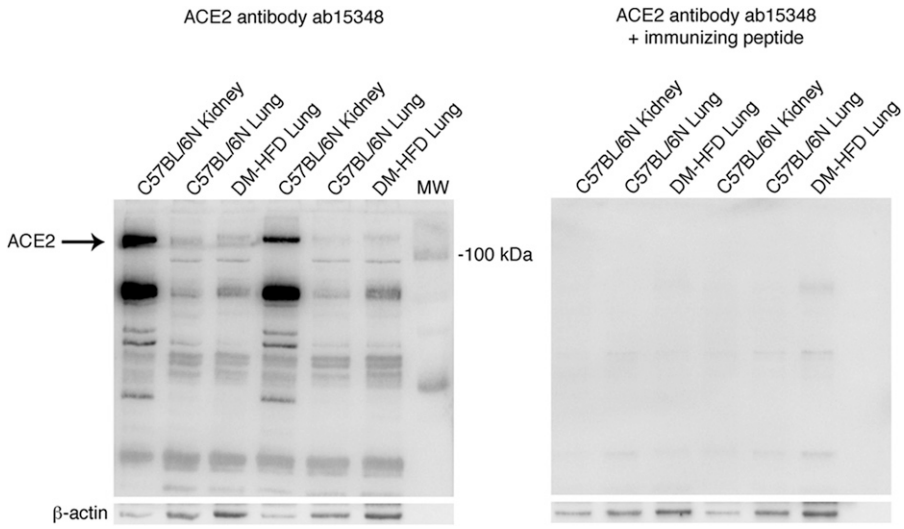

Figure 2—Specificity of the ACE2 antibody (ab15348). Western blotting of kidney and lung samples from male C57BL/6N mice (aged ~9 weeks) and lung samples from aged, DM-HFD mice (male C57BL/6 mice fed an HFD for a total of 36 weeks and receiving an intraperitoneal injection of STZ after 15 weeks of HFD). Shown are Western blotting with the polyclonal ACE2 antibody alone (left) and Western blotting of the same samples with the polyclonal ACE2 antibody preincubated with immunizing peptide (CKGENNPGFQNTDDVQTSF) (right).

Given that *Ace2* is primarily expressed in the bronchioles of mouse lungs, we next explored the possibility that *Ace2* expression could be changed by RAS blockade specifically in alveolar cells without affecting overall transcript levels in lung homogenates. We chose to study type II pneumocytes because these cells have been shown to contain SARS-CoV-2 virus particles in infected humans (31), and we isolated primary type II pneumocytes using Dynabeads colabeled with antibodies directed against epithelial cell adhesion molecule and surfactant protein C. Confirming enrichment for isolated type II pneumocytes, we observed an ~1,000-fold enrichment for the gene encoding surfactant protein C (*Sftpc*) in the primary cells compared with unrelated control cells (primary cultured kidney fibroblasts) (Fig. 3*K*). As we had seen in whole-lung tissue, there was no change in *Ace2* mRNA levels in type II pneumocytes of mice treated with either ramipril or telmisartan (Fig. 3*L*).

Generation of RAS Blocker–Treated, Aged, Diabetic HFD-Fed Mice

Next, we queried whether either ACE2 or TMPRSS2 mRNA or protein levels are affected by diabetic comorbidity either alone or with RAS blockade. We did this by studying ramipril- or telmisartan-treated, aged, diabetic HFD-fed (DM-HFD) mice, along with age-matched controls (Fig. 4*A*). Among the DM-HFD mice, body weight declined after STZ administration (mean ± SD: before STZ 42.2 ± 3.2 g, 19 weeks after STZ 34.5 ± 9.6 g [$n = 20$], $P < 0.01$ by Student *t* test) such that there was no overall difference in body weight between age-matched controls and DM-HFD mice at the end of the study period (Fig. 4*B*). As expected, blood glucose (Fig. 4*C* and *D*) and plasma cholesterol (Fig. 4*E*) were higher in DM-HFD mice than in age-matched controls, whereas plasma triglycerides did not differ between groups (Fig. 4*F*). SBP was reduced equivalently with ramipril and telmisartan in DM-HFD mice after 2 weeks of treatment (Fig. 4*G*), and consistent with the short duration of treatment, whereas urine albumin excretion (Fig. 4*H*) and glomerulosclerosis index (Fig. 4*I*) were increased in DM-HFD mice, they were unaffected by either ramipril or telmisartan (Fig. 4*H* and *I*).

Lung ACE2 and TMPRSS2 Protein Levels Are Increased in DM-HFD Mice and Unaffected by RAS Blockade, and TMPRSS2 Is Upregulated in the Kidneys of Telmisartan-Treated DM-HFD Mice

By immunoblotting, we observed that both ACE2 and TMPRSS2 protein levels were higher in the lungs of DM-HFD mice than in age-matched controls (Fig. 5*A* and *B*), whereas mRNA levels were unaltered across the four treatment groups (Fig. 5*C* and *D*). As we had observed in young C57BL/6N mice, neither ramipril nor telmisartan affected ACE2 or TMPRSS2 expression in the lungs of DM-HFD mice (Fig. 5*A–D*). In the kidneys, ACE2 protein levels (but not mRNA levels) were similarly higher in DM-HFD mice than age-matched controls (Fig. 5*E* and *G*). In contrast, TMPRSS2 protein (Fig. 5*F*) and mRNA (Fig. 5*H*) levels tended to be higher in RAS blocker–treated DM-HFD mice and were significantly increased with telmisartan treatment, without change in transcript distribution as determined by in situ hybridization (Fig. 6). On review of *Tmprss2* in situ hybridization, however, we also noted that distal nephron RNAscope puncta appeared sparser in age-matched controls (Fig. 6) than we had earlier

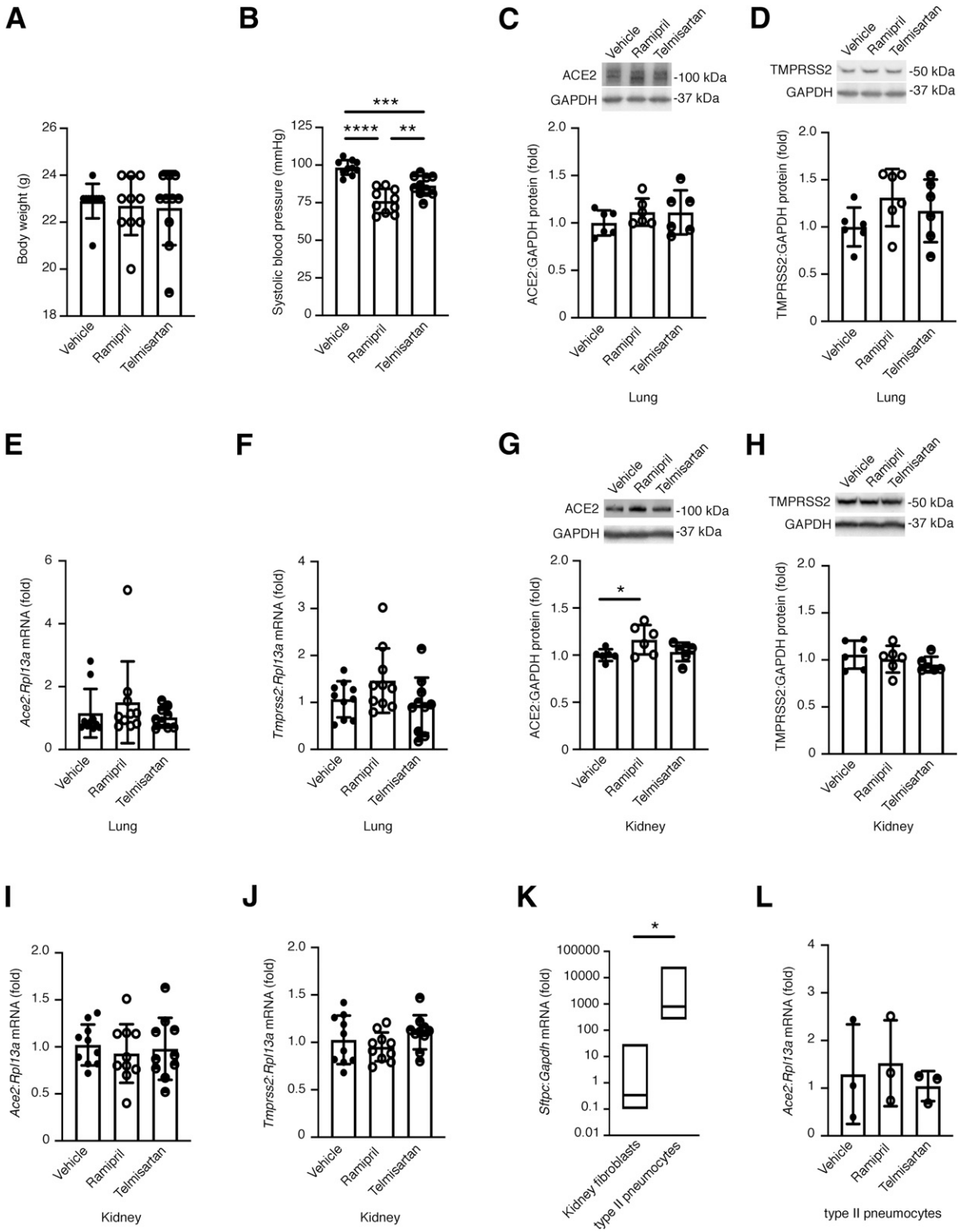

Figure 3—RAS blockade has minimal effect on lung and kidney ACE2 and TMPRSS2 in young otherwise healthy mice. Male C57BL/6N mice aged 7–8 weeks were randomly allocated to receive standard drinking water or the ACE inhibitor ramipril (10 mg/kg/day) or the AT1 receptor blocker (ARB) telmisartan (3 mg/kg/day) for 1 week. *A*: Body weight ($n = 10$/group). *B*: SBP ($n = 10$/group). *C* and *D*: Immunoblotting for ACE2 and TMPRSS2 in mouse lungs ($n = 6$/group). *E* and *F*: qRT-PCR for *Ace2* and *Tmprss2* in mouse lungs ($n = 10$/group, except *Ace2* in C57BL/6N + telmisartan where $n = 9$). *G* and *H*: Immunoblotting for ACE2 and TMPRSS2 in mouse kidneys ($n = 6$/group). *I* and *J*: qRT-PCR for *Ace2* and *Tmprss2* in mouse kidneys ($n = 10$/group). *K*: qRT-PCR for the type II pneumocyte marker *Sftpc* in primary mouse lung type II pneumocytes compared with a control cell not expected to express *Sftpc* (kidney fibroblasts) ($n = 3$/group). *L*: qRT-PCR for *Ace2* in primary type II pneumocytes ($n = 3$/group). Data are mean ± SD, except in panel *K*, which shows median, maximum, and minimum. $^*P < 0.05$, $^{**}P < 0.01$, $^{***}P < 0.001$, $^{****}P < 0.0001$ by one-way ANOVA followed by Fisher least significant difference post hoc test for more than two groups or two-tailed Student *t* test for two-group comparison.

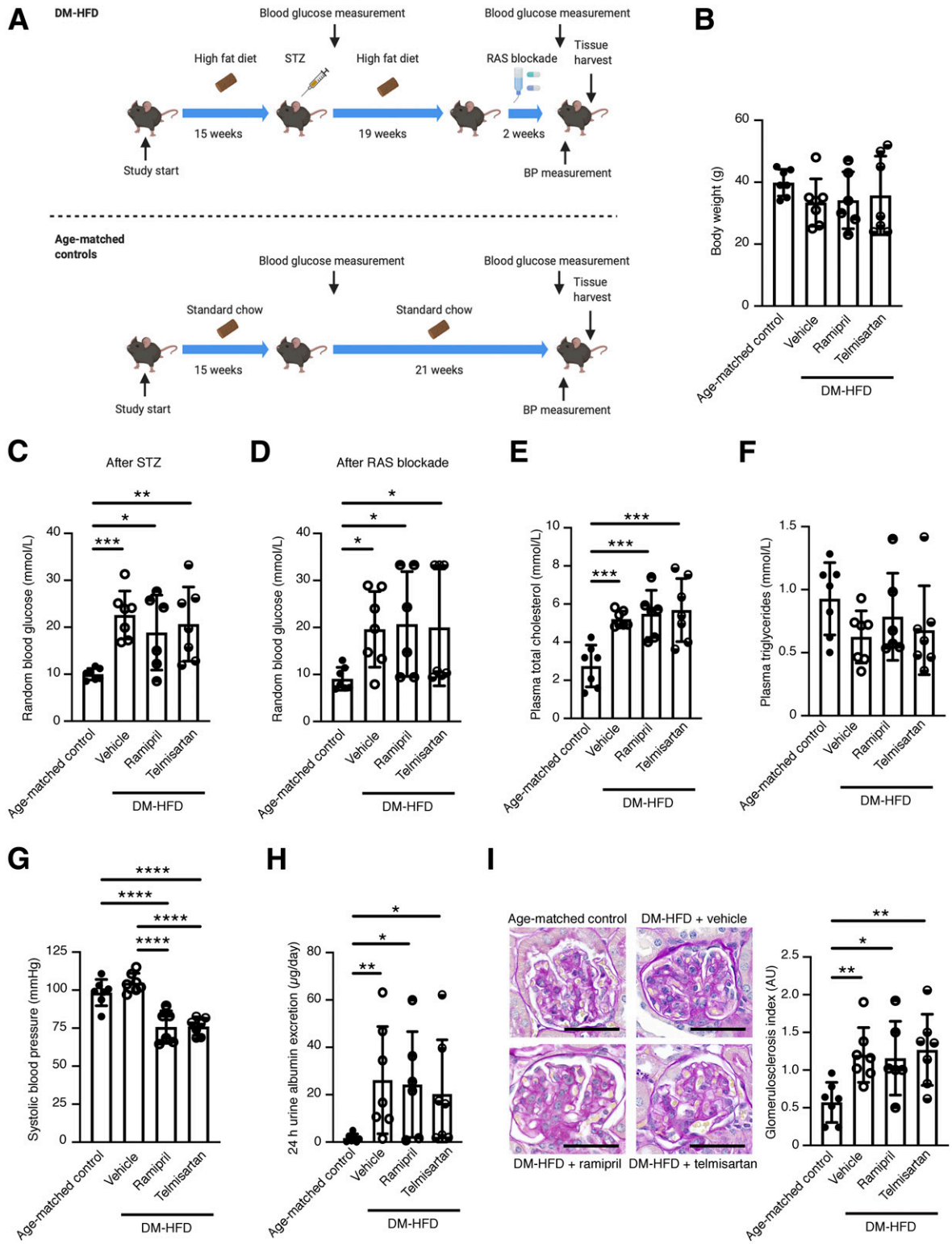

Figure 4—Phenotypic characterization of male aged, DM-HFD mice. *A*: Timeline for DM-HFD mouse generation. Mice were fed an HFD for 15 weeks, received an intraperitoneal injection of STZ (90 mg/kg), and were maintained on an HFD for a further 19 weeks before receiving ramipril (10 mg/kg/day) or telmisartan (3 mg/kg/day) in drinking water or drinking water alone for 2 further weeks. Male age-matched controls were given standard chow and standard drinking water throughout the study period and did not receive STZ. Age-matched controls, $n = 7$; DM-HFD + vehicle, $n = 7$; DM-HFD + ramipril, $n = 6$; and DM-HFD + telmisartan, $n = 7$. *B*: Body weight. *C*: Blood glucose 2 weeks after STZ administration. *D*: Blood glucose 2 weeks after RAS blockade. *E–H*: Plasma cholesterol, plasma triglycerides, SBP, and urine albumin excretion at the end of the study period. *I*: Representative periodic acid Schiff–stained kidney sections (magnification ×400 [scale bars = 50 μm]) and semiquantitative glomerulosclerosis index. Data are mean ± SD. *$P < 0.05$, **$P < 0.01$, ***$P < 0.001$, ****$P < 0.0001$ by one-way ANOVA followed by Fisher least significant difference post hoc test (*C*, *E*, *G*, and *I*) or Kruskal-Wallis test with Dunn posttest (*D* and *H*). AU, arbitrary unit; BP, blood pressure.

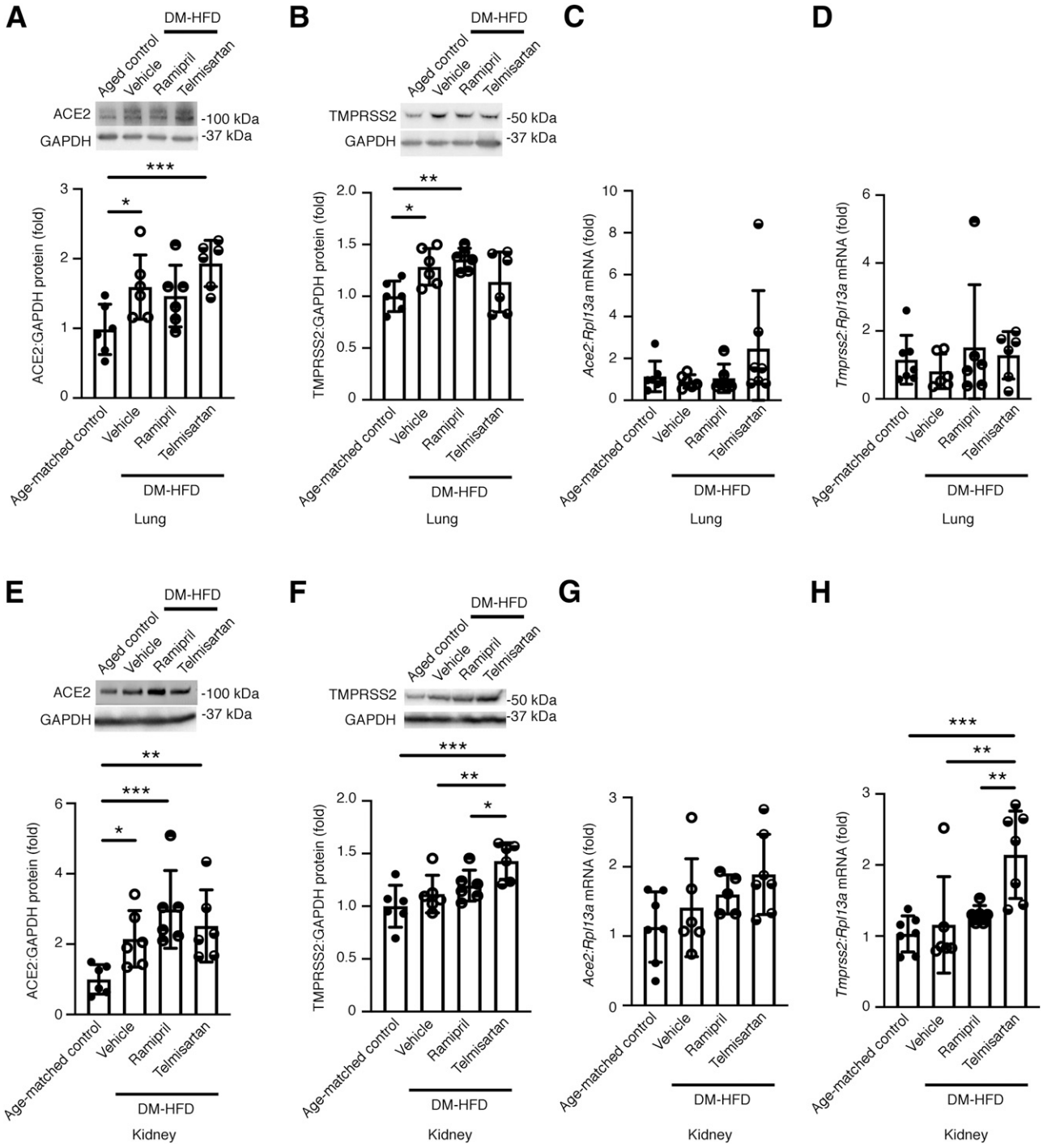

Figure 5— Lung and kidney ACE2 are upregulated in male aged, DM-HFD mice, and kidney TMPRSS2 expression is increased in telmisartan-treated DM-HFD mice. Ramipril (10 mg/kg/day) or telmisartan (3 mg/kg/day) were dosed to aged, DM-HFD mice for 2 weeks. *A* and *B*: Immunoblotting for ACE2 and TMPRSS2 in mouse lungs ($n = 6$/group). *C*: qRT-PCR for *Ace2* in mouse lungs. Age-matched controls, $n = 7$; DM-HFD + vehicle, $n = 6$; DM-HFD + ramipril, $n = 6$; and DM-HFD + telmisartan, $n = 7$. *D*: qRT-PCR for *Tmprss2* in mouse lungs. Age-matched controls, $n = 7$; DM-HFD + vehicle, $n = 6$; DM-HFD + ramipril, $n = 6$; DM-HFD + telmisartan, $n = 6$. *E* and *F*: Immunoblotting for ACE2 and TMPRSS2 in mouse kidneys ($n = 6$/group). *G*: qRT-PCR for *Ace2* in mouse kidneys. Age-matched controls, $n = 7$; DM-HFD + vehicle, $n = 6$; DM-HFD + ramipril, $n = 5$; and DM-HFD + telmisartan, $n = 7$. *H*: qRT-PCR for *Tmprss2* in mouse kidneys. Age-matched controls, $n = 7$; DM-HFD + vehicle, $n = 6$; DM-HFD + ramipril, $n = 6$; and DM-HFD + telmisartan, $n = 7$. Data are mean ± SD. $^*P < 0.05$, $^{**}P < 0.01$, $^{***}P < 0.001$ by one-way ANOVA followed by Fisher least significant difference post hoc test.

seen in young healthy male mice (Fig. 1). This prompted us to quantitatively compare qRT-PCR–derived mRNA levels between young male C57BL/6N mice and nondiabetic aged controls, and in doing so, we observed a significant diminution in both *Ace2* and *Tmprss2* in the kidneys but not in the lungs of aged mice (Supplementary Fig. 1).

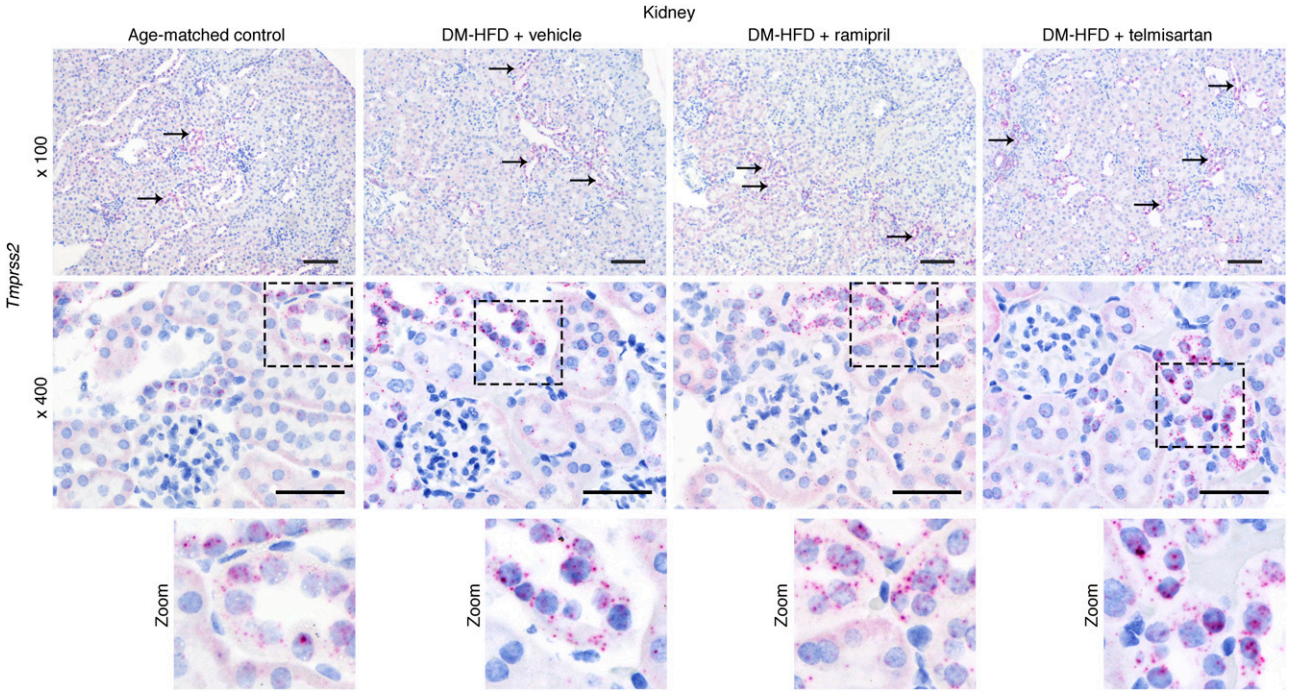

Figure 6—Predominant expression of *Tmprss2* in distal nephron segments in the kidney cortices of RAS blocker–treated, aged, DM-HFD mice. Ramipril (10 mg/kg/day) or telmisartan (3 mg/kg/day) were dosed to aged DM-HFD mice for 2 weeks. RNAscope in situ hybridization for *Tmprss2* (top magnification ×100 [scale bars = 100 μm], bottom magnification ×400 [scale bars = 50 μm]). The arrows label some of the kidney tubules in each section that contain red RNAscope puncta in the lower magnification (×100) images. The zoomed-in images are enlargements of the boxed areas in the higher magnification (×400) images.

Lung ACE2 Activity Is Increased With Age and Diabetic Comorbidity but Not With RAS Blockade

Finally, given that the lungs are the primary sites of SARS-CoV-2 infection and given that we had observed an increase in ACE2 protein in the lungs of DM-HFD mice that was unaffected by RAS blockade, we decided to use LC-MS/MS to further explore the possibility that lung ACE2 activity is upregulated in the setting of diabetic comorbidity. Because adverse COVID-19 outcomes are more common in males than females (32), in aged individuals (3), and in people with diabetes (33), we elected to perform the analysis across six mouse groups chosen to mimic these clinical scenarios: young (9 weeks of age) male C57BL/6N mice, young female C57BL/6N mice, aged mice (44 weeks of age), aged DM-HFD mice, and aged DM-HFD mice treated with ramipril or telmisartan. Table 1 shows the levels of six RAS metabolites [Ang II (1–8), Ang 1–7, Ang I (1–10), Ang III (2–8), Ang 1–5, and Ang IV (3–8)] reported individually for each mouse in the study. Ang II was the predominant angiotensin in mouse lungs, with quantifiable levels of Ang III (2–8) in most samples that closely correlated with Ang II levels ($r^2 = 0.93$, $P < 0.0001$ by simple linear regression).

To measure ACE2 activity in mouse lungs, samples of homogenized tissue were spiked with Ang II before measurement of Ang 1–7 levels in the presence and absence of the ACE2 inhibitor MLN-4760, with the difference between the two samples being considered specific for ACE2 activity (Fig. 7*A*). There was no difference in lung ACE2 activity between male and female mice. In contrast, there was a stepwise increase in lung ACE2 activity in aged control mice and aged DM-HFD mice (DM-HFD vs. aged control, $P = 0.0632$), with lung ACE2 activity being significantly higher in DM-HFD mice than young controls (Fig. 7*B*). Neither ramipril nor telmisartan affected lung ACE2 activity in DM-HFD mice (Fig. 7*B*).

DISCUSSION

Herein, we report the results of a reverse translational survey examining some of the risk factors associated with adverse outcomes from COVID-19. Among the observations, two stand out as being of immediate translational importance. First, levels of two host proteins important for viral entry (i.e., ACE2, TMPRSS2) are upregulated in the lungs of diabetic mice that mimic host factors linked to severe COVID-19. Second, despite using multiple different experimental modalities, we were unable to detect any effect of RAS blockade on the levels of lung ACE2 or TMPRSS2 in mice with comorbid diabetes. The findings provide biological insights into the causes of increased risk of severe COVID-19, and they provide biological reassurance for the continued use of RAS blockers in people with diabetes who remain at the same increased risk of noninfectious complications during the pandemic as they did before.

To address the question of whether lung or kidney ACE2 or TMPRSS2 may be altered in comorbid diabetes, we focused our experiments on the study of aged, HFD-fed

Table 1—RAS metabolites in the lungs of young (9 weeks of age) male and female C57BL/6N mice, aged mice (44 weeks of age), and male aged, DM-HFD mice treated with vehicle or ramipril (10 mg/kg/day) or telmisartan (3 mg/kg/day) for 2 weeks

	Ang II (1–8) (fmol/g)	Ang 1–7 (fmol/g)	Ang I (1–10) (fmol/g)	Ang III (2–8) (fmol/g)	Ang 1–5 (fmol/g)	Ang IV (3–8) (fmol/g)
Male C57BL/6N						
Mouse 1	32.1	<8	9.6	7.9	<3	<2
Mouse 2	24.2	<8	<4	5.5	<3	<2
Mouse 3	30.4	<8	<4	4.7	<3	2.4
Mouse 4	16.4	<8	<4	5.4	3.2	<2
Mouse 5	25.2	<8	<4	7.9	<3	<2
Mean ± SD	25.7 ± 6.7	–	–	–	–	–
Female C57BL/6N						
Mouse 6	13.3	<8	<4	<4	<3	<2
Mouse 7	27.9	<8	<4	12.7	4.2	2.7
Mouse 8	28.9	<8	<4	12.1	<3	<2
Mouse 9	17.8	<8	<4	7.4	<3	<2
Mouse 10	18.4	<8	<4	4.4	<3	<2
Mean ± SD	21.3 ± 6.8	–	–	–	–	–
Aged control						
Mouse 11	73.5	<8	<4	21.4	<3	3.3
Mouse 12	62.8	<8	<4	18.3	<3	<2
Mouse 13	142.6	<8	7.9	40.3	7.1	6.4
Mouse 14	31.9	<8	<4	13.5	<3	<2
Mouse 15	64.6	<8	<4	17.2	<3	<2
Mean ± SD	75.1 ± 40.9[a,b]	–	–	–	–	–
DM-HFD + vehicle						
Mouse 16	162.5	<8	10.5	42.9	13.3	9.2
Mouse 17	22.5	<8	<4	6.3	<3	2.1
Mouse 18	73.1	<8	4.5	20.9	6.3	<2
Mouse 19	77.5	<8	9.9	15.4	8.5	2.3
Mouse 20	17.8	<8	<4	<4	3.8	<2
Mean ± SD	70.7 ± 58.3[a,b]	–	–	–	–	–
DM-HFD + ramipril						
Mouse 21	23.9	<8	26.7	5.5	11.1	<2
Mouse 22	12.3	<8	16.7	<4	<3	<2
Mouse 23	25.7	<8	45.3	<4	<3	<2
Mouse 24	2.2	<8	<4	<4	<3	<2
Mouse 25	14.3	<8	<4	<4	<3	<2
Mean ± SD	15.7 ± 9.6[c,d]	–	–	–	–	–
DM-HFD + telmisartan						
Mouse 26	8.4	<8	<4	<4	<3	<2
Mouse 27	5.7	<8	<4	<4	<3	<2
Mouse 28	36.6	<8	<4	<4	<3	4.0
Mouse 29	24.6	<8	<4	<4	<3	2.2
Mouse 30	103.1	18.6	30.9	23.5	15.8	8.0
Mean ± SD	35.7 ± 39.7	–	–	–	–	–

[a]$P < 0.05$ vs. male C57BL/6N. [b]$P < 0.05$ vs. female C57BL/6N. [c]$P < 0.05$ vs. aged control. [d]$P < 0.05$ vs. DM-HFD + vehicle by one-way ANOVA followed by Fisher least significant difference post hoc test.

mice with STZ-induced diabetes. We selected this model because questions have been raised over the ability of monogenic models of diabetes to mimic the complex multifactorial and progressive natural history of diabetes in humans (34). Furthermore, we initiated RAS blockade in aged, DM-HFD mice after a prolonged period of follow-up (42 weeks of age) to mimic the circumstances in which treatment may be initiated in patients with established comorbid diabetes. However, despite our efforts to mimic the human diabetes phenotype, it should be acknowledged that STZ is not a physiological means of diabetes induction. The findings should thus be considered alongside observations made in other mouse models, for instance, the recent description that RAS blockade does not affect lung or kidney ACE2 in healthy mice (17) or that kidney ACE2 protein levels are upregulated in *db/db* mice and in otherwise healthy mice 7 weeks after STZ administration (12). In the opinion of the authors, the most salient finding in the current study is the comparison of lung ACE2 activity derived by LC-MS/MS in the aged, DM-HFD mouse model. This experiment enabled several intrinsic comparisons: no difference in lung ACE2 activity between healthy young

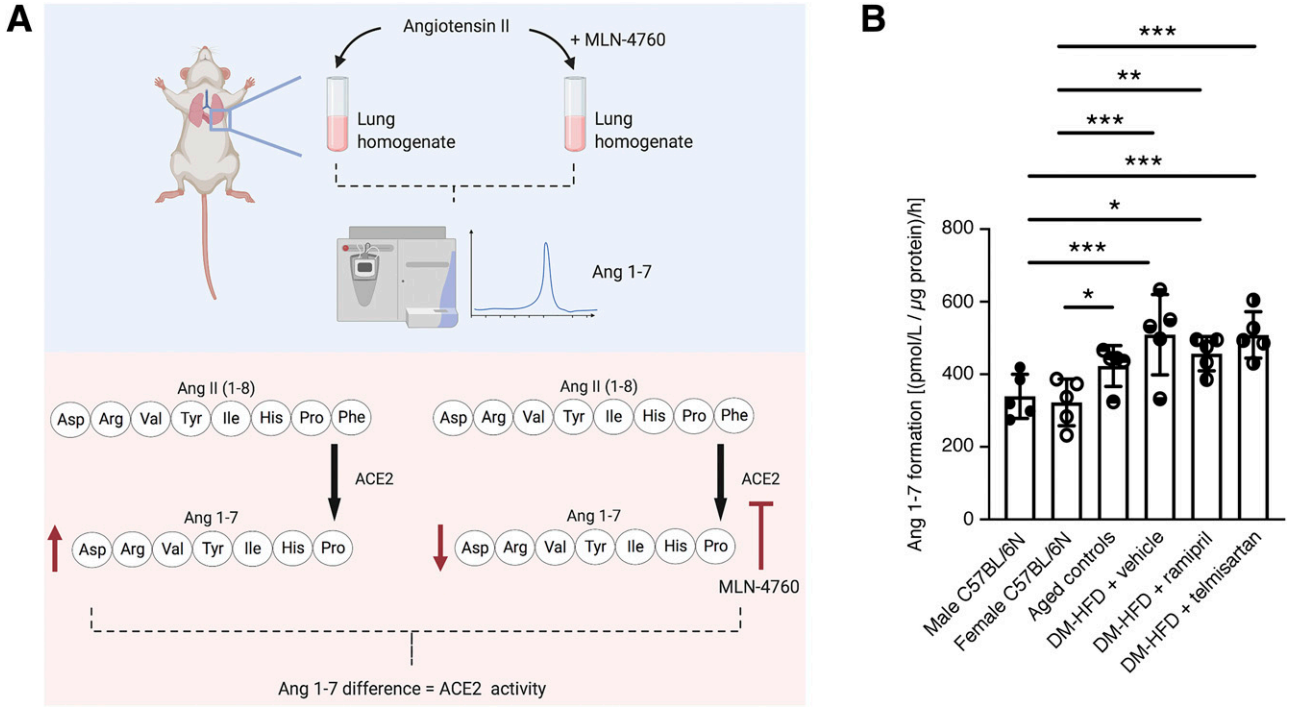

Figure 7— Lung ACE2 activity is increased in aged, DM-HFD mice and is unaffected by RAS blockade. Mice were fed an HFD for 15 weeks, received an intraperitoneal injection of STZ (90 mg/kg), and were maintained on an HFD for a further 19 weeks before receiving ramipril (10 mg/kg/day) or telmisartan (3 mg/kg/day) in drinking water or drinking water alone for 2 further weeks. Male age-matched controls were given standard chow and standard drinking water throughout the study period and did not receive STZ. Male C57BL/6N and female C57BL/6N mice were 9 weeks of age and had received standard chow and standard drinking water. *A*: Schematic illustrating the method for determination of lung ACE2 activity by LC-MS/MS. *B*: Lung ACE2 activity ($n = 5$/group). Data are mean ± SD. $^{*}P < 0.05$, $^{**}P < 0.01$, $^{***}P < 0.001$ by one-way ANOVA followed by Fisher least significant difference post hoc test.

male and female mice, a stepwise increase with aging and diabetic comorbidity, no influence on this increase by either an ACE inhibitor (ramipril) or ARB (telmisartan), and no difference in lung ACE2 activity between ramipril and telmisartan.

The increase in lung ACE2 activity in aged, DM-HFD mice, without change in mRNA levels, is aligned with earlier assertions made in mouse kidneys (12) and recent observations made in lung tissue of humans with type 2 diabetes (35) that increased ACE2 protein or activity in diabetes is regulated at the posttranscriptional level. Indeed, a recent best research practices review article similarly emphasized the importance of the posttranscriptional regulation of ACE2 in determining its protein abundance (36). A number of factors influence the expression level of a protein beyond transcript abundance, including translation rates, translation rate modulation, modulation of protein half-life (including the ubiquitin-proteasome system or autophagy), protein synthesis delay and protein transport (37), and, in the case of ACE2, potentially microRNAs (38) and protein shedding (39).

In mouse lungs, ACE2 and TMPRSS2 expression patterns mirrored each other (being upregulated at the protein level with comorbid diabetes and being unaffected by RAS blockade), although their site-specific patterns of expression differed. We observed that *Ace2* transcripts were primarily (albeit not exclusively) present in the bronchioles, whereas *Tmprss2* expression was more diffuse. In the kidneys, we similarly observed a difference in *Ace2* and *Tmprss2* transcript distribution, *Ace2* being primarily expressed in the proximal tubules and *Tmprss2* being predominantly localized to the distal nephron. Single-cell RNA sequencing data of human kidney tissue have also revealed this disparity in the localization of *ACE2* (predominantly proximal tubule) and *TMPRSS2* (predominantly distal nephron) (40). These differences underscore that although ACE2 and TMPRSS2 are often considered together in the context of COVID-19 (18) and the two proteins have previously been reported to interact (30), they likely do not have a major teleological relationship. Indeed, knockout of *Tmprss2* yields no discernible phenotype (41), and outside of virology, TMPRSS2 has primarily been linked to prostate cancer (42).

The significance of the transcriptional upregulation of TMPRSS2 in the kidneys of DM-HFD mice treated with RAS blockade, particularly telmisartan, is currently unclear. This is especially the case given the age-related decline in both *Ace2* and *Tmprss2* we observed in the kidneys of nondiabetic mice. On the one hand, *Tmprss2* is primarily (although not exclusively) localized to the

distal nephron (and transitional epithelium), and coronavirus-like particles have been detected in distal tubule cells from postmortem tissue of patients with COVID-19 (11). On the other hand, viral S protein cleavage may be achieved by several different host proteases other than TMPRSS2 (e.g., furin, trypsin, cathepsins, TMPRSS4, and human airway trypsin-like protease [43]). TMPRSS2 upregulation may represent a physiological response to local ion transport changes at the level of the distal tubule and cortical collecting duct induced by RAS blockade, and it may or may not influence SARS-CoV-2 viral entry and kidney outcomes in patients with COVID-19. Alternatively, the serine protease inhibitor camostat, which inhibits TMPRSS2 and is undergoing clinical trial as a treatment for COVID-19 (44), has historically shown itself to attenuate proteinuria in patients with diabetic kidney disease (45). In sum, we present these findings to inform knowledge given the urgency of the pandemic but counsel caution in their interpretation at the present time.

Our study has limitations. First, the patterns and changes in expression of ACE2 or TMPRSS2 may differ between mice and humans. In this regard, we identified prominent expression of both *Ace2* and *Tmprss2* in mouse bronchioles, whereas comparable in situ hybridization of human lungs has shown *TMPRSS2* transcript in the bronchiolar epithelium with low (albeit detectable) levels of *ACE2* in the bronchioles (46). In contrast, single-cell analyses in human lung tissue have produced variable results, describing *ACE2* primarily in bronchial transitory secretory cells (47), bronchiolar basal cells, club cells and ciliated cells and type II pneumocytes (48), and type II pneumocytes and ciliated cells (49). Second, although we studied the effects of both an ACE inhibitor (ramipril) and an ARB (telmisartan), dosing of the two agents was based on previous publications that reported a significant reduction in SBP in mice (20,21) and was not designed to necessarily achieve equivalence. Third, we used LC-MS/MS to compare ACE2 activity between study groups, unearthing an increase in ACE2 activity in the lungs of aged, DM-HFD mice that was unaffected by RAS blockade. However, the relative contribution of ACE2 to lung Ang II metabolism in general may not be substantial. For instance, ACE2 activity in the current study was determined on the basis of Ang 1–7 formation in mouse lung tissue spiked with exogenous Ang II. Recently, it was reported that the major carboxypeptidase responsible for the formation of Ang 1–7 in mouse lungs is prolyl oligopeptidase, not ACE2 (15). However, this was accounted for in the assay we used by the inclusion of the prolyl oligopeptidase inhibitor Z-pro-prolinal. Along the same lines, when we measured RAS metabolites in mouse lungs by LC-MS/MS, we observed generally higher levels of Ang III (2–8) than Ang 1–7, suggesting an important role for aminopeptidase A in mouse lung Ang II metabolism, which cleaves Ang II to form Ang III (2–8). It also warrants reemphasis that, at least in mice, ACE2 protein is at best lowly expressed in lung tissue, certainly compared with the kidneys. Finally, some epidemiological studies have not found an association between RAS blockade and increased risk from COVID-19 (50). However, long-term RAS blockade has also been linked to increased risk of acute kidney injury among patients with severe COVID-19 (51). The present findings add biological context to these observations and extend them farther. We observed no difference in the effect on ACE2 expression or activity between an ACE inhibitor and an ARB despite the theoretically different mechanisms that this may occur and despite an upregulation in ACE2 that occurs with comorbid diabetes.

In summary, lung and kidney ACE2 is upregulated in diabetic mice that mimic some of the host factors associated with adverse COVID-19 outcomes. This upregulation is due to intrinsic characteristics associated with diabetic comorbidity and is not due to RAS blocker therapy.

Acknowledgments. The graphical abstract (in Supplementary Material) and Figs. 4*A* and 7*A* were created with BioRender.com.

Funding. H.K. is a recipient of a Kidney Foundation of Canada KRESCENT postdoctoral fellowship. V.G.Y. is a recipient of a Diabetes Canada postdoctoral fellowship. A.A. is a recipient of a Diabetes Canada Diabetes Investigator Award and holds the Keenan Chair in Medicine at St. Michael's Hospital and University of Toronto. These studies were supported, in part, by grants from the Heart and Stroke Foundation of Canada (G-17-0018231), the Canadian Institutes of Health Research (PJT153284 and PJT166083), and the RDV Foundation.

Duality of Interest. These studies were supported, in part, by a grant from Boehringer Ingelheim. T.K. is an employee of Boehringer Ingelheim. T.K. and A.A. are named as inventors on a patent by Boehringer Ingelheim for the use of dipeptidyl peptidase 4 inhibition in the treatment of heart failure. A.A. has received research support from Boehringer Ingelheim and AstraZeneca; has participated in advisory boards for Abbott, Dexcom, Boehringer Ingelheim/Eli Lilly, and Novo Nordisk; and has received an unrestricted educational grant from Eli Lilly. No other potential conflicts of interest relevant to this article were reported.

Author Contributions. S.N.B., H.K., and V.G.Y. designed and performed the experiments, analyzed the data, and revised and edited the manuscript. S.L.A. performed histological experiments. M.G.K. performed hemodynamic assessments and analyzed the data. Y.L. performed RNA isolations and analyzed the data. T.K. coordinated the mass spectrometry experiments. A.A. designed the experiments, analyzed the data, supervised the study, and wrote the manuscript. A.A. is guarantor of this work and, as such, had full access to all the data in the study and takes responsibility for the integrity of the data and the accuracy of the data analysis.

References

1. Li B, Yang J, Zhao F, et al. Prevalence and impact of cardiovascular metabolic diseases on COVID-19 in China. Clin Res Cardiol 2020;109:531–538

2. Wu C, Chen X, Cai Y, et al. Risk factors associated with acute respiratory distress syndrome and death in patients with coronavirus disease 2019 pneumonia in Wuhan, China. JAMA Intern Med 2020;180:934–943

3. Zhou F, Yu T, Du R, et al. Clinical course and risk factors for mortality of adult inpatients with COVID-19 in Wuhan, China: a retrospective cohort study. Lancet 2020;395:1054–1062

4. Barron E, Bakhai C, Kar P, et al. Associations of type 1 and type 2 diabetes with COVID-19-related mortality in England: a whole-population study. Lancet Diabetes Endocrinol 2020;8:813–822

5. Shang J, Ye G, Shi K, et al. Structural basis of receptor recognition by SARS-CoV-2. Nature 2020;581:221–224

6. Yan R, Zhang Y, Li Y, Xia L, Guo Y, Zhou Q. Structural basis for the recognition of SARS-CoV-2 by full-length human ACE2. Science 2020;367:1444–1448

7. Wang Q, Zhang Y, Wu L, et al. Structural and functional basis of SARS-CoV-2 entry by using human ACE2. Cell 2020;181:894–904.e9

8. Lan J, Ge J, Yu J, et al. Structure of the SARS-CoV-2 spike receptor-binding domain bound to the ACE2 receptor. Nature 2020;581:215–220
9. Ferrario CM. ACE2: more of Ang-(1-7) or less Ang II? Curr Opin Nephrol Hypertens 2011;20:1–6
10. Drucker DJ. Coronavirus infections and type 2 diabetes-shared pathways with therapeutic implications. Endocr Rev 2020;41:bnaa011
11. Su H, Yang M, Wan C, et al. Renal histopathological analysis of 26 post-mortem findings of patients with COVID-19 in China. Kidney Int 2020;98:219–227
12. Wysocki J, Ye M, Soler MJ, et al. ACE and ACE2 activity in diabetic mice. Diabetes 2006;55:2132–2139
13. Lores E, Wysocki J, Batlle D. ACE2, the kidney and the emergence of COVID-19 two decades after ACE2 discovery. Clin Sci (Lond) 2020;134:2791–2805
14. Ye M, Wysocki J, William J, Soler MJ, Cokic I, Batlle D. Glomerular localization and expression of angiotensin-converting enzyme 2 and angiotensin-converting enzyme: implications for albuminuria in diabetes. J Am Soc Nephrol 2006;17: 3067–3075
15. Serfozo P, Wysocki J, Gulua G, et al. Ang II (angiotensin II) conversion to angiotensin-(1-7) in the circulation is POP (prolyloligopeptidase)-dependent and ACE2 (angiotensin-converting enzyme 2)-independent. Hypertension 2020;75: 173–182
16. Fang L, Karakiulakis G, Roth M. Are patients with hypertension and diabetes mellitus at increased risk for COVID-19 infection? Lancet Respir Med 2020;8:e21
17. Wysocki J, Lores E, Ye M, Soler MJ, Batlle D. Kidney and lung ACE2 expression after an ACE inhibitor or an Ang II receptor blocker: implications for COVID-19. J Am Soc Nephrol 2020;31:1941–1943
18. Hoffmann M, Kleine-Weber H, Schroeder S, et al. SARS-CoV-2 cell entry depends on ACE2 and TMPRSS2 and is blocked by a clinically proven protease inhibitor. Cell 2020;181:271–280.e8
19. Zuk A, Palevsky PM, Fried L, et al. Overcoming translational barriers in acute kidney injury: a report from an NIDDK workshop. Clin J Am Soc Nephrol 2018;13: 1113–1123
20. Otto A, Fontaine J, Berkenboom G. Ramipril treatment protects against nitrate-induced oxidative stress in eNOS-/- mice: an implication of the NADPH oxidase pathway. J Cardiovasc Pharmacol 2006;48:842–849
21. Fujisaka S, Usui I, Kanatani Y, et al. Telmisartan improves insulin resistance and modulates adipose tissue macrophage polarization in high-fat-fed mice. Endocrinology 2011;152:1789–1799
22. Yuen DA, Stead BE, Zhang Y, et al. eNOS deficiency predisposes podocytes to injury in diabetes. J Am Soc Nephrol 2012;23:1810–1823
23. Kaur H, Takefuji M, Ngai CY, et al. Targeted ablation of periostin-expressing activated fibroblasts prevents adverse cardiac remodeling in mice. Circ Res 2016; 118:1906–1917
24. Hinton AO Jr., Yang Y, Quick AP, et al. SRC-1 regulates blood pressure and aortic stiffness in female mice. PLoS One 2016;11:e0168644
25. Wang F, Flanagan J, Su N, et al. RNAscope: a novel in situ RNA analysis platform for formalin-fixed, paraffin-embedded tissues. J Mol Diagn 2012;14:22–29
26. Advani A, Connelly KA, Yuen DA, et al. Fluorescent microangiography is a novel and widely applicable technique for delineating the renal microvasculature. PLoS One 2011;6:e24695
27. Zheng YY, Ma YT, Zhang JY, Xie X. COVID-19 and the cardiovascular system. Nat Rev Cardiol 2020;17:259–260
28. Kuba K, Imai Y, Rao S, et al. A crucial role of angiotensin converting enzyme 2 (ACE2) in SARS coronavirus-induced lung injury. Nat Med 2005;11:875–879
29. Warner FJ, Lew RA, Smith AI, Lambert DW, Hooper NM, Turner AJ. Angiotensin-converting enzyme 2 (ACE2), but not ACE, is preferentially localized to the apical surface of polarized kidney cells. J Biol Chem 2005;280:39353–39362
30. Heurich A, Hofmann-Winkler H, Gierer S, Liepold T, Jahn O, Pöhlmann S. TMPRSS2 and ADAM17 cleave ACE2 differentially and only proteolysis by TMPRSS2 augments entry driven by the severe acute respiratory syndrome coronavirus spike protein. J Virol 2014;88:1293–1307
31. Yao XH, He ZC, Li TY, et al. Pathological evidence for residual SARS-CoV-2 in pulmonary tissues of a ready-for-discharge patient. Cell Res 2020;30:541–543
32. Du Y, Tu L, Zhu P, et al. Clinical features of 85 fatal cases of COVID-19 from Wuhan. A retrospective observational study. Am J Respir Crit Care Med 2020;201: 1372–1379
33. CDC COVID-19 Response Team. Preliminary estimates of the prevalence of selected underlying health conditions among patients with coronavirus disease 2019 - United States, February 12-March 28, 2020. MMWR Morb Mortal Wkly Rep 2020;69:382–386
34. Drucker DJ. Never waste a good crisis: confronting reproducibility in translational research. Cell Metab 2016;24:348–360
35. Wijnant SRA, Jacobs M, Van Eeckhoutte HP, et al. Expression of ACE2, the SARS-CoV-2 receptor, in lung tissue of patients with type 2 diabetes. Diabetes 2020;69:2691–2699
36. Sparks MA, South AM, Badley AD, et al. Severe acute respiratory syndrome coronavirus 2, COVID-19, and the renin-angiotensin system: pressing needs and best research practices. Hypertension 2020;76:1350–1367
37. Liu Y, Beyer A, Aebersold R. On the dependency of cellular protein levels on mRNA abundance. Cell 2016;165:535–550
38. Widiasta A, Sribudiani Y, Nugrahapraja H, Hilmanto D, Sekarwana N, Rachmadi D. Potential role of ACE2-related microRNAs in COVID-19-associated nephropathy. Noncoding RNA Res 2020;5:153–166
39. Palau V, Pascual J, Soler MJ, Riera M. Role of ADAM17 in kidney disease. Am J Physiol Renal Physiol 2019;317:F333–F342
40. Batlle D, Soler MJ, Sparks MA, et al.; COVID-19 and ACE2 in Cardiovascular, Lung, and Kidney Working Group. Acute kidney injury in COVID-19: emerging evidence of a distinct pathophysiology. J Am Soc Nephrol 2020;31:1380–1383
41. Kim TS, Heinlein C, Hackman RC, Nelson PS. Phenotypic analysis of mice lacking the Tmprss2-encoded protease. Mol Cell Biol 2006;26:965–975
42. Lin B, Ferguson C, White JT, et al. Prostate-localized and androgen-regulated expression of the membrane-bound serine protease TMPRSS2. Cancer Res 1999; 59:4180–4184
43. Ou X, Liu Y, Lei X, et al. Characterization of spike glycoprotein of SARS-CoV-2 on virus entry and its immune cross-reactivity with SARS-CoV. Nat Commun 2020; 11:1620
44. Nitulescu GM, Paunescu H, Moschos SA, et al. Comprehensive analysis of drugs to treat SARS-CoV-2 infection: mechanistic insights into current COVID-19 therapies (Review). Int J Mol Med 2020;46:467–488
45. Matsubara M, Taguma Y, Kurosawa K, Hotta O, Suzuki K, Ishizaki M. Effect of camostat mesilate for the treatment of advanced diabetic nephropathy. J Lab Clin Med 1990;116:206–210
46. Hou YJ, Okuda K, Edwards CE, et al. SARS-CoV-2 reverse genetics reveals a variable infection gradient in the respiratory tract. Cell 2020;182:429–446.e14
47. Lukassen S, Chua RL, Trefzer T, et al. SARS-CoV-2 receptor ACE2 and TMPRSS2 are primarily expressed in bronchial transient secretory cells. EMBO J 2020;39:e105114
48. Sungnak W, Huang N, Bécavin C, et al.; HCA Lung Biological Network. SARS-CoV-2 entry factors are highly expressed in nasal epithelial cells together with innate immune genes. Nat Med 2020;26:681–687
49. Ziegler CGK, Allon SJ, Nyquist SK, et al.; HCA Lung Biological Network. Electronic address:lung-network@humancellatlas.org; HCA Lung Biological Network. SARS-CoV-2 receptor ACE2 is an interferon-stimulated gene in human airway epithelial cells and is detected in specific cell subsets across tissues. Cell 2020;181:1016–1035.e19
50. de Abajo FJ, Rodríguez-Martín S, Lerma V, et al.; MED-ACE2-COVID19 Study Group. Use of renin-angiotensin-aldosterone system inhibitors and risk of COVID-19 requiring admission to hospital: a case-population study. Lancet 2020;395: 1705–1714
51. Oussalah A, Gleye S, Clerc Urmes I, et al. Long-term ACE inhibitor/ARB use is associated with severe renal dysfunction and acute kidney injury in patients with severe COVID-19: results from a referral center cohort in the Northeast of France. Clin Infect Dis 2020;71:2447–2456